scientific data

Check for updates

OPEN

DATA DESCRIPTOR

A multi-modal dataset of electroencephalography and functional near-infrared spectroscopy recordings for motor imagery of multi-types of joints from unilateral upper limb

Weibo Yi[1,3] ✉, Jiaming Chen[2,3], Dan Wang[2] ✉, Xinkang Hu[2], Meng Xu[2], Fangda Li[2], Shuhan Wu[2] & Jin Qian[2]

As one of the important brain-computer interface (BCI) paradigms, motor imagery (MI) enables the control of external devices via identification of motor intention by decoding the features of Electroencephalography (EEG). Movement imagination of multi-types of joints from the same limb allows the development of more accurate and intuitive BCI systems. In this work, we reported an open dataset including EEG and functional near-infrared spectroscopy (fNIRS) recordings from 18 subjects performing eight MI tasks from four types of joints including hand open/close, wrist flexion/extension, wrist abduction/adduction, elbow pronation/supination, elbow flexion/extension, shoulder pronation/supination, shoulder abduction/adduction, and shoulder flexion/extension, resulting in a total of 5760 trials. The validity of multi-modal data was verified both from the EEG/fNIRS activation patterns and the classification performance. It is expected that this dataset will facilitate the development and innovation of decoding algorithms for MI of multi-types of joints based on multi-modal EEG-fNIRS data.

Background & Summary

Brain computer interface (BCI) is a system that enables communication between the brain and computers via brain signals like Electroencephalography (EEG) without peripheral nerves and muscles, and it can be applied in fields of rehabilitation, entertainment[1], etc. Motor Imagery based BCI (MI-BCI) is one of the most important BCI paradigms, and it enables identification of motor intention by decoding MI induced EEG (MI-EEG) collected by electrodes placed on the scalp. Conventional MI-BCI studies focus on motor intention of simple limbs (e.g. left hand, right hand, or foot)[2] or the combination of limbs (e.g. both hands)[3]. However, there is often a cognitive disconnect between the MI tasks performed and the corresponding actions of the output device. For instance, tasks like left- and right-hand MI are intuitive for controlling horizontal movement, but using feet or tongue MI for vertical movement lacks a clear mental connection to the device's action. This results in unnatural and less effective control tasks, especially in high-dimensional paradigms. Therefore, techniques like MI decoding of multiple joints from the same limb are being developed to make the control more natural and intuitive[4]. In recent years, a number of studies aiming at MI decoding of different joints of the same limb have emerged[5]. Usually, the MI decoding of hand[6], wrist[4], elbow[7], and shoulder[8] from unilateral upper limb is the main topic of this field. The movements include hand open/close[9], wrist flexion/extension[10], elbow flexion/extension[11], elbow pronation/supination[12] (also noted as forearm pronation/supination[13] as they correspond to the same joint),

[1]Beijing Institute of Mechanical Equipment, Beijing, 100854, China. [2]College of Computer Science, Beijing University of Technology, Beijing, 100124, China. [3]These authors contributed equally: Weibo Yi, Jiaming Chen. ✉e-mail: yiweibo1987@163.com; wangdan@bjut.edu.cn

shoulder flexion/extension, shoulder pronation/supination, and shoulder abduction/adduction[14]. Multi-types of joints MI decoding enables more intuitive communication with devices, which is beneficial for building more accurate interaction systems.

In MI decoding studies, public datasets usually provide a benchmark for evaluating the performance of data-driven methods based on machine learning and deep learning, which play a key role in research on decoding algorithms[15]. For instance, the BCI Competition IV Dataset IIa and IIb[16] were employed frequently in MI decoding studies that focus on algorithm improvements for motor intention detection of limbs (e.g., left/right hand, foot, and tongue). Both datasets were released in the 4th BCI Competition with MI-EEG of 9 subjects. Also, datasets including EEG data collected from more subjects (e.g., the OpenBMI dataset[17] have attracted more attention because they can better reveal the generalization capability of algorithms across multiple subjects. To achieve more intuitive motor control, open EEG datasets involving MI tasks of different joints from the same limb have emerged in recent years. For instance, Ofner *et al*. released an open-available dataset including MI-EEG of 15 subjects with MI tasks of elbow flexion/extension, wrist supination/pronation, and hand close/open[18]. Ma *et al*. proposed a public dataset including 25 subjects performing hand and elbow tasks[19]. Bi *et al*. published a dataset collected from experiments with 10 healthy right-handed subjects performing six upper limb motor imagery tasks (elbow flexion/extension, forearm supination/pronation, hand open/close) that contains 18,000 trials of EEG data recorded via 16 electrodes (500 Hz, 10–20 system)[20]. However, existing public datasets only cover MI tasks of joints like hand, wrist, and elbow, while MI tasks of shoulder movements are absent in these datasets. Furthermore, these MI datasets only possess EEG recordings, while functional near-infrared spectroscopy (fNIRS) recordings are expected to provide complementary MI-related information in hemodynamic activity without electro-optical interference[21]. Also, compared with standalone EEG methods, stronger performance of multi-modal EEG-fNIRS decoding methods were reported in recent years[22]. Therefore, we proposed an free access dataset containing simultaneously collected EEG and fNIRS recordings during 8 MI tasks of 4 types of joints (i.e., hand, wrist, elbow, and shoulder) from unilateral upper limb. This dataset can be employed for evaluating performance of methods on MI decoding of different joints, in order to facilitate the development of MI-BCI.

In this work, we collected EEG and fNIRS recordings simultaneously from 18 subjects performing eight MI tasks of four types of joints including hand, wrist, elbow, and shoulder from the right upper limb. The eight MI tasks were hand open/close, wrist flexion/extension, wrist abduction/adduction, elbow pronation/supination, elbow flexion/extension, shoulder pronation/supination, shoulder abduction/adduction, and shoulder flexion/extension. There are 320 trials (with 40 trials per MI task) for each subject with a total of 5760 trials of EEG and fNIRS data in our dataset. The raw recordings were provided in this dataset for the convenience of both data analysis and further use for evaluating the performance of decoding algorithms.

To validate the effect of the data, we performed preliminarily time-frequency and topographical analysis on the simultaneously collected EEG-fNIRS data. Meanwhile, we verified the discriminability by using typical deep-learning and machine-learning methods to distinguish different joints in 2-class scenario. The highest classification accuracy of 65.49% was achieved between hand open/close and shoulder pronation/supination using EEG data by applying a typical deep learning-based method ShallowConvNet[23] with data augmentation of white noise adding.

The dataset proposed in this work can provide a benchmark for evaluating the performance of decoding algorithms trained for identifying the motor intention of different joints from the same limb. It is expected to facilitate the development of data-driven methods designed for both standalone EEG and multi-modal EEG-fNIRS hybrid MI-BCI systems.

Methods

Subjects. All the experiments conducted in this study were approved by the ethical committee of Tianjin University (approved number: TJUE-210). The experiment was performed according to the Declaration of Helsinki. Data in the experiment were collected from 18 right-handed healthy individuals (8 males and 10 females), aged between 22 and 27 years, who had no prior experience with MI-BCI. Subjects in the experiment were required to have no prior neurological or psychiatric conditions and have normal vision or vision corrected to normal, and they were asked to avoid consuming alcohol, tea, and coffee on the day of the experiment as well as the day before. Before the experiment, all participants signed the informed consent. To ensure anonymity, we assigned aliases to all subjects, referring to them as "subject1" to "subject18". Prior to recording, subjects were required to take one session for the training, consisting of 8 blocks (with the first 2 blocks of motor execution and the remaining 6 blocks of motor imagery) for their familiarization and proper understanding of the tasks.

Experimental paradigm. The participants were seated comfortably in a chair, with their hands resting naturally on their thighs, and their eyes kept one meter away from the screen. The time scheme of the experiment is shown in Fig. 1. Each trial (18–20 seconds) began with a white fix cross at the center of the monitor for 2 seconds. Then, a text cue and a video cue appeared in the screen for 2 seconds, reminding the subjects of the upcoming task. Next, the video cue disappeared with the text cue unchanged, and the text of "Start Imagining" appeared, asking the subject to imagine the target movement for 4 seconds using kinesthetic imagery rather than visual imagery. During MI execution, each subject was instructed to suppress blinking (to prevent eye movement artifacts) and swallowing (to prevent muscle artifacts) to minimize electrooculogram (EOG) and electromyogram (EMG) artifacts. After the task period, the word "Rest" appeared on the screen for 10–12 seconds randomly. Because of the inherent delays in hemodynamic responses, we used a long resting period to avoid the corruption of fNIRS data from two consecutive trials. During the rest period, subjects were encouraged to relax but minimize any eye movements and refrain from muscle activity.

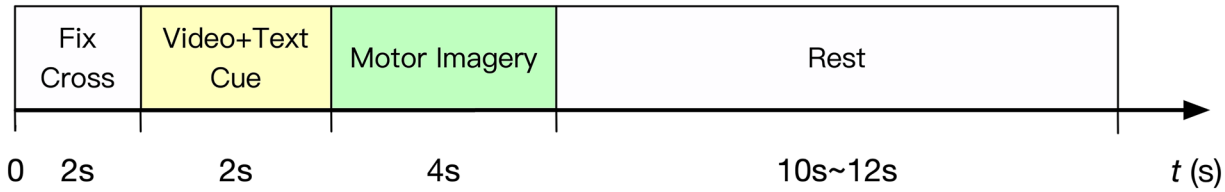

Fig. 1 Time scheme of the experiment.

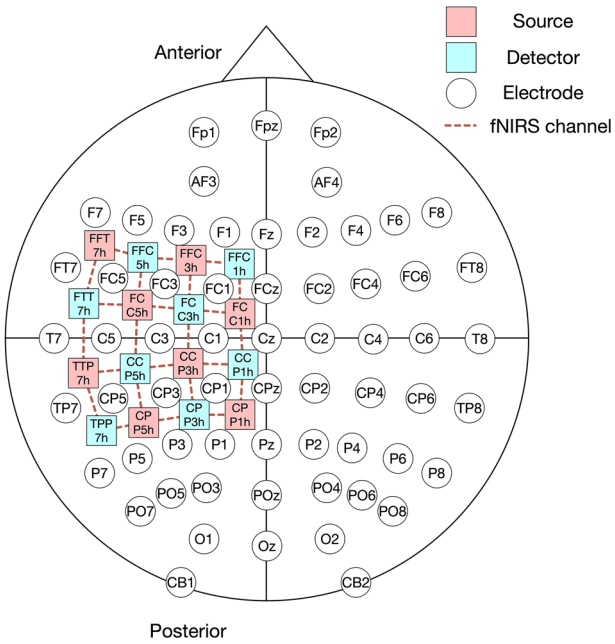

Fig. 2 The location of EEG electrodes, fNIRS sources, and fNIRS detectors.

For each subject, 8 motor tasks (i.e., hand open/close, wrist flexion/extension, wrist abduction/adduction, elbow pronation/supination, elbow flexion/extension, shoulder pronation/supination, shoulder abduction/adduction, and shoulder flexion/extension) from the right upper limb were performed, and the EEG-fNIRS data were collected simultaneously in one session. A session contains 8 blocks, with 40 trials in each block (5 trials for each task). The sequence of trials in each block were randomized. There was a 5 to 10 minutes break between each block for the subject. Therefore, there are 320 trials for each subject in the dataset, with a total of 5760 trials.

Data collection and preprocessing. In this dataset, EEG and fNIRS data were acquired simultaneously, and we designed the experiment according to the frequently employed practice in this field on EEG[5,19] and fNIRS[24]. The location of electrodes (EEG), sources (fNIRS), and detectors (fNIRS) were shown in Fig. 2, where red squares, blue squares, white circles, and red dash lines stand for fNIRS sources, fNIRS detectors, EEG electrodes, and fNIRS channels, respectively. EEG data were collected using a 64-channel electrode cap covering the whole brain and the Neuroscan SynAmps2 amplifier (Neuroscan, Inc.) with the sampling frequency set at 1000 Hz. The left mastoid (M1) was employed as the reference during the EEG measurements, and electrode impedances were maintained below 10 kΩ throughout the experiment. During data acquisition, a 50 Hz notch filter were employed to remove power line interference, and a band-pass filter of 0.5–100 Hz was selected to cover the entire EEG frequency range, including the alpha and beta bands mainly related to motor imagery. Regarding fNIRS, the NIRScout system (NIRx GmbH, Berlin, Germany) with 8 sources and 8 detectors were employed to collect fNIRS data at a sampling rate of 7.8125 Hz. The optodes (i.e., 8 sources and 8 detectors) were placed at the left hemisphere according to the international 10-5 system on the same recording cap, arranged in a 8×8 grid, with each adjacent source-detector pair denoting one fNIRS channel (shown in red dash line in Fig. 2). This configuration resulted in 24 channels, enabling more detailed monitoring of cortical activity associated with the right upper limb.

The preprocessing of data was performed with the MNE-Python library[25]. For EEG data, we employed the common average reference (CAR) method to remove the impact of the reference electrode and a 3rd order Butterworth band-pass filter of 4–40 Hz to focus on the relevant frequency bands (i.e., 4–40 Hz for general brain activity covering motor rhythms of theta, mu, beta, and low gamma) and remove high-frequency EMG noise (typically above 50 Hz) as well as low-frequency drift (below 0.5 Hz). To reduce the computational cost, the data were then downsampled to 250 Hz. For fNIRS data, we first calculated the concentration changes of Oxygenated Hemoglobin (HbO) and Deoxygenated Hemoglobin (HbR) with the modified Beer-Lambert law[26].

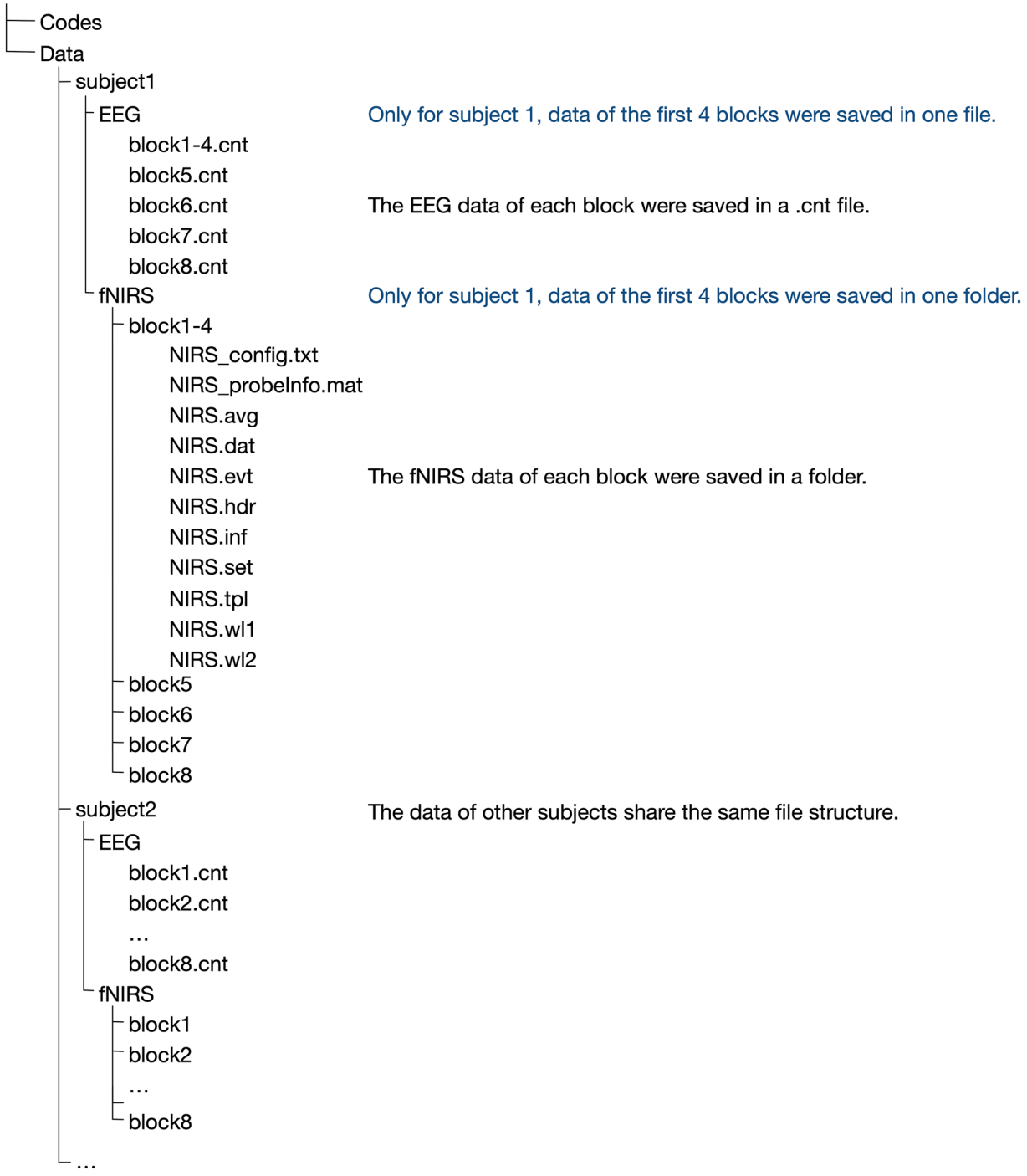

Fig. 3 The structure of EEG and fNIRS data files.

Then, a 6th order Butterworth band-pass filter with passband of 0.01–0.1 Hz was employed to remove artifacts such as heartbeat (1∼1.5 Hz), respiration (0.2∼0.5 Hz), and Mayer waves (∼0.1 Hz).

Data Records

The data records have been released in a figshare repository[27], which is openly accessible. We provided the raw recordings of EEG and fNIRS, and the structure of the raw files is shown in Fig. 3. The files were organized by subjects, with EEG folder and fNIRS folder containing two kinds of signals respectively.

In the EEG folder, the data and metadata of EEG were saved in a "cnt" file, and the name of files denotes the block number. If loaded by the EEGLAB toolbox of MATLAB, a structure variable called "EEG" can be obtained. It contains key properties of nbchan, srate, pnts, data, chanlocs, and events, which stand for the number of channels, the sampling rate, the number of sampling points, the collected data, the name of channels, and the information of events (MI task type, etc.), respectively. In the "event" property, triggers of numbers from 1 to 8 stand

for hand open/close, wrist flexion/extension, wrist abduction/adduction, elbow pronation/supination, elbow flexion/extension, shoulder pronation/supination, shoulder abduction/adduction, and shoulder flexion/extension, respectively. Note that the first four blocks of EEG data from subject 1 were saved in one file, while the EEG data of each block from other subjects were saved in different files separately.

In the fNIRS folder, the data of fNIRS from each block were saved in a folder named with the block number. In each folder, "NIRS.wl1" and "NIRS.wl2" stand for two wavelengths of light recorded in raw light intensity units (i.e., the raw data of fNIRS), and "NIRS.evt" contains the trigger information (type and time stamp). In the "NIRS.evt" file, triggers of numbers from 1.0 to 8.0 stand for hand open/close, wrist flexion/ extension, wrist abduction/adduction, elbow pronation/supination, elbow flexion/extension, shoulder pronation/supination, shoulder abduction/adduction, and shoulder flexion/extension, respectively. The "NIRS_probeInfo.mat" stand for the 3D scalp-level optode coordinates and channel list for the recording's montage. Note that the first four blocks of fNIRS data from subject 1 were saved in one folder, while the fNIRS data of each block from other subjects were saved in different folders separately.

Technical Validation

EEG Validation. The event-related spectral perturbation (ERSP) method was used to inspect the spectral power changes of MI-EEG from time-frequency domain. Baseline-normalized ERSP values (dB) were calculated from −4 s to 6 s with the time interval of −4s to −2s as the baseline. The averaged time-frequency maps of all subjects at electrode C3 were plotted for each task because all the MI tasks in this work are from the right upper limb. In addition, topographical maps based on the ERSP values from 60 electrodes (except HEO,VEO, CB1, and CB2) by averaging the ERSP values within the corresponding frequency bands (i.e., 8–13 Hz for alpha band and 13–30 Hz for beta band) and time intervals (from 0 to 4 s).

The time-frequency maps are shown in Fig. 4, where the three dash lines stand for the time of cue shown, the start of MI, and the end of MI, respectively. The maps show clear and long-lasting power decrease in both alpha (12–13 Hz) and beta (20–25 Hz) bands during task period for all MI tasks. Also, stronger ERD patterns in tasks from hand, wrist, and elbow are found compared with those in tasks from shoulder.

The topographical maps of alpha band and beta band are shown in Figs. 5, 6 respectively. The ERD patterns present apparent contralateral dominances for each MI task in alpha band, concentrated in the motor areas. However, the difference of spatial distribution in alpha band between each task is not quite apparent. Regarding the spatial distribution in beta band, stronger ERD patterns can be observed at left motor area in tasks of hand and elbow, while those from tasks of wrist and shoulder are slightly weaker. These results suggest that the activation at contralateral motor areas was induced by performing MI tasks of four types of joints from the right upper limb, which is consistent with the neurophysiological basis[28].

Moreover, in order to validate the discriminability of different joints in MI tasks using EEG data, a typical deep learning-based method called ShallowConvNet[23] with the white noise addition data augmentation[29] was employed in an intra-subject 5-fold cross-validation experiment. We used the one-vs-one strategy in 2-class scenario and conducted 28 pairs of classification between two different MI tasks. The results are shown in Table 1, where HOC, WFE, WAA, EPS, EFE, SPS, SAA, and SFE stand for hand open/close, wrist flexion/extension, wrist abduction/adduction, elbow pronation/supination, elbow flexion/extension, shoulder pronation/supination, shoulder abduction/adduction, and shoulder flexion/extension, respectively. The results for each classification were above the chance level (50%) in the 2-class scenario. We sorted the classification accuracy in descending order. Highest classification performance of 65.49% can be observed in the classification of MI tasks between hand and shoulder. This reveals more apparent feature discriminability of MI tasks between hand and shoulder, whose spatial distance of cortical areas is biggest among all MI tasks. Overall, the classification of hand-shoulder, wrist-shoulder, and hand-elbow tasks achieved higher accuracy found in top-10 results. Besides, inferior results were found in the classification of hand-wrist, wrist-elbow, and elbow-shoulder tasks, which may result from the quite similar patterns of MI-EEG from more adjacent somatotopic regions. In addition to Convolutional Neural Networks-based methods like ShallowConvNet, future improvements can be achieved by the attention mechanism[30] and Transformer-based networks[31]. These techniques have been successfully used in MI decoding and other fields, which are helpful for improving the decoding performance with collected EEG data.

fNIRS Validation. Increasing in HbO and minor reductions in HbR are usually considered as typical indications of cortical activation[32] for fNIRS signals. In fNIRS-based MI decoding, the time courses of relative concentration changes of HbO and HbR around the C3 position were frequently used for analyzing the MI-related activation of right-hand task[26]. Therefore, we calculated the mean concentration changes of HbO and HbR of four channels around the C3 location (i.e., CCP3h-FCC3h, CCP3h-CCP5h, FCC5h-CCP5h, and FCC5h-FCC3h) with the time interval of −4s to −2s as the baseline. Averaged concentration changes of HbO and HbR across 18 subjects are shown in Fig. 7 where the dash line indicates the start of MI. The increase of concentration changes of HbO can be seen clearly during the MI period (0–4 s) for all tasks, and the peak can be achieved during the rest period after MI because of the inherent delays in hemodynamic responses. The variation of HbO concentration from each task shows similar trend, but the peak amplitude differed between different MI tasks. Regarding the spatial difference, the topographical map of concentration of HbO averaged from 8 s to 10s[22] (around the peak value of HbO concentration) were plotted. As shown in Fig. 8, the spatial distribution of HbO concentration varies from different MI tasks. Obvious activity can be observed around C1 and C3 location in hand and wrist tasks, while the distribution of HbO concentration weakens around C3 and gradually converges to C1 in elbow and shoulder tasks, which is consistent with the somatotopic organization of different joints.

Furthermore, to demonstrate the separability of fNIRS data, we performed an intra-subject 5-fold cross-validation experiment. Similar to the experiment on EEG data, we conducted 28 pairs of classification

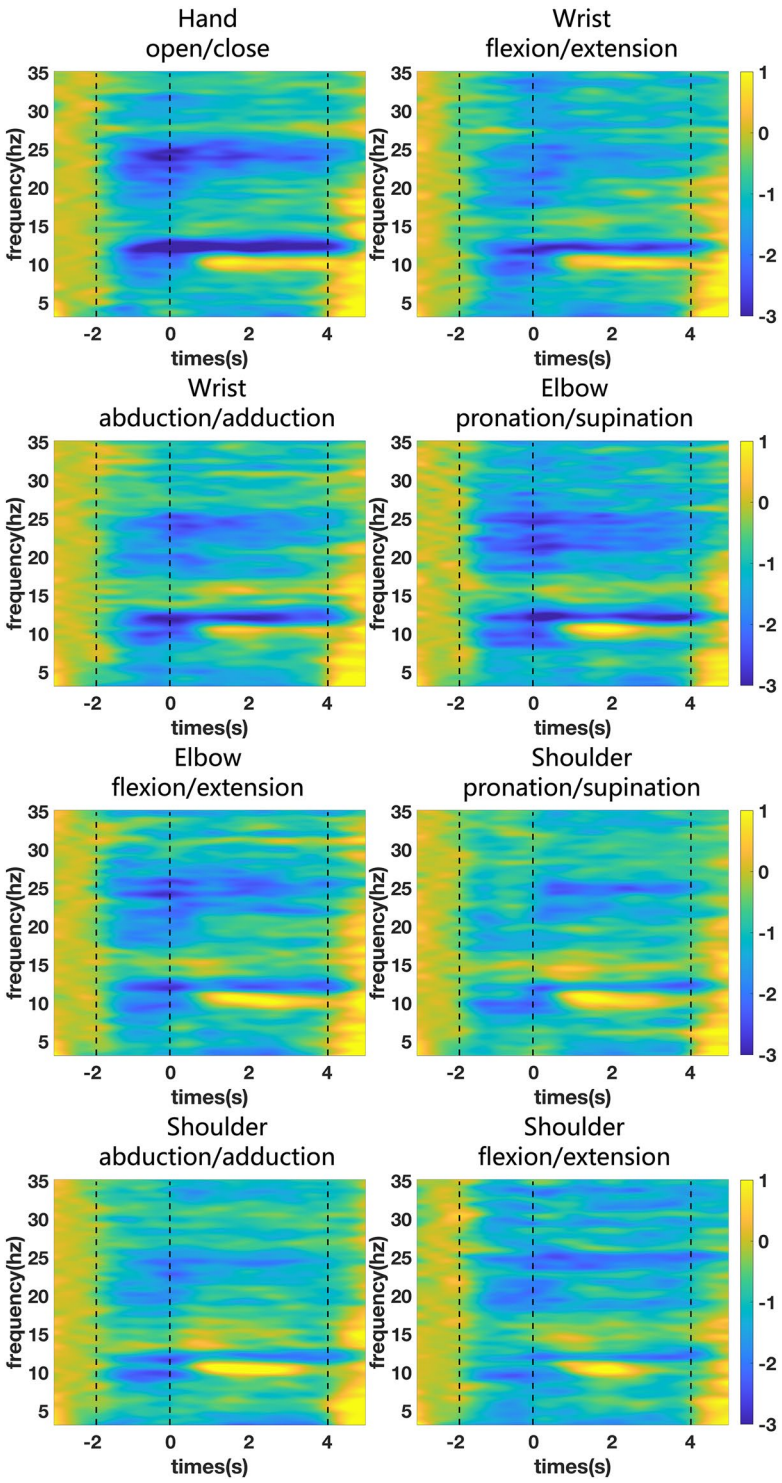

Fig. 4 The time-frequency maps for 8 MI tasks averaged across all subjects.

between two different MI tasks with the one-vs-one strategy. We extracted the mean and slope of HbO and HbR as temporal features and classified them via the support vector machine (SVM) algorithm, which is a widely used method in MI decoding[33]. To account for the delay in hemodynamic activity[24], accuracy was calculated for a 4-second sliding window (same as the length of the MI period) with a step of 1 s from 0 to 15 s. We recorded the best accuracy among different slices for each classification between 2 tasks. The result is shown in Table 2, where HOC, WFE, WAA, EPS, EFE, SPS, SAA, and SFE stand for hand open/close, wrist flexion/extension, wrist abduction/adduction, elbow pronation/supination, elbow flexion/extension, shoulder pronation/supination, shoulder abduction/adduction, and shoulder flexion/extension, respectively. The results for each classification were above the chance level (50%) in the 2-class scenario. The classification results of fNIRS were

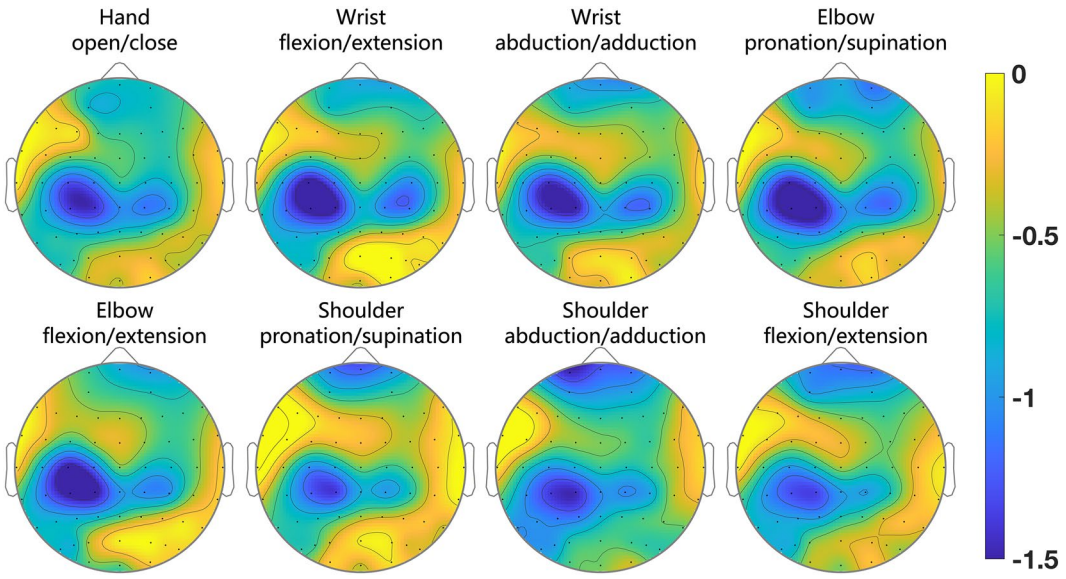

Fig. 5 The topographical distribution of power in α band for 8 MI tasks averaged across all subjects.

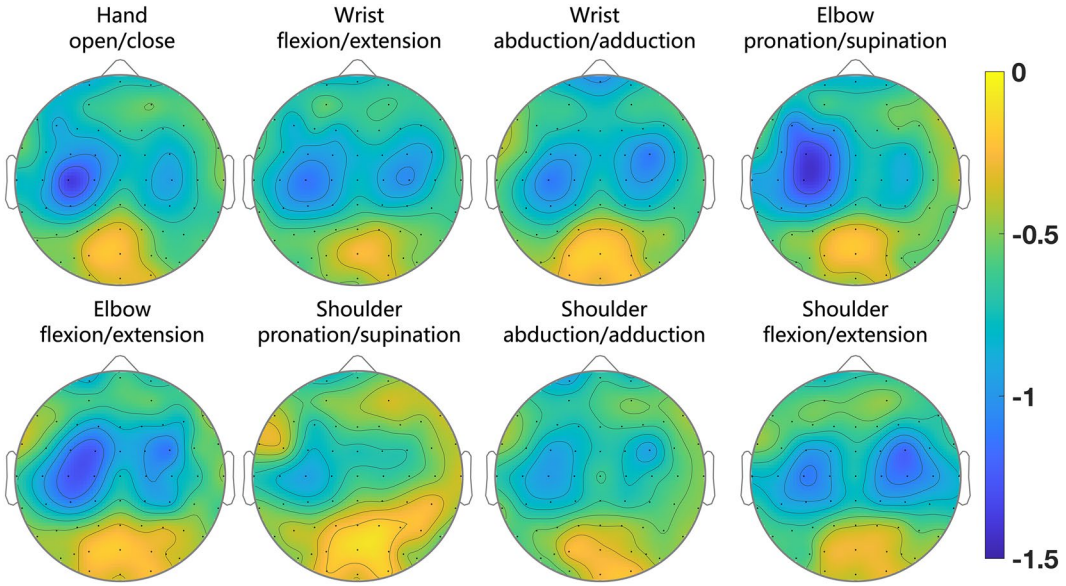

Fig. 6 The topographical distribution of power in β band for 8 MI tasks averaged across all subjects.

Tasks	Acc. (%)	Tasks	Acc. (%)	Tasks	Acc. (%)	Tasks	Acc. (%)
HOC/SPS	65.49	SPS/SFE	59.97	WAA/EFE	57.85	HOC/EPS	56.32
HOC/SFE	63.37	WAA/SPS	59.72	SPS/SAA	57.36	WFE/EPS	56.25
HOC/SAA	63.13	WFE/SAA	59.44	HOC/WAA	56.88	SAA/SFE	56.02
WFE/SPS	61.81	EPS/SPS	59.24	WFE/WAA	56.88	HOC/WFE	55.90
HOC/EFE	61.18	EPS/SFE	58.97	EFE/SAA	56.88	EPS/SAA	55.69
WFE/SFE	61.14	EFE/SPS	58.61	WAA/SFE	56.83	EPS/EFE	53.89
WAA/SAA	60.56	EFE/SFE	58.23	WFE/EFE	56.60	WAA/EPS	52.22

Table 1. The mean accuracy (%) of ShallowConvNet with noise addition data augmentation on EEG data of 18 subjects in an intra-subject 5-fold cross-validation experiment in 2-class scenario. Acc. means accuracy. "A/B" stand for the classification between task A and B. HOC, WFE, WAA, EPS, EFE, SPS, SAA, and SFE stand for hand open/close, wrist flexion/extension, wrist abduction/adduction, elbow pronation/supination, elbow flexion/extension, shoulder pronation/supination, shoulder abduction/adduction, and shoulder flexion/extension, respectively.

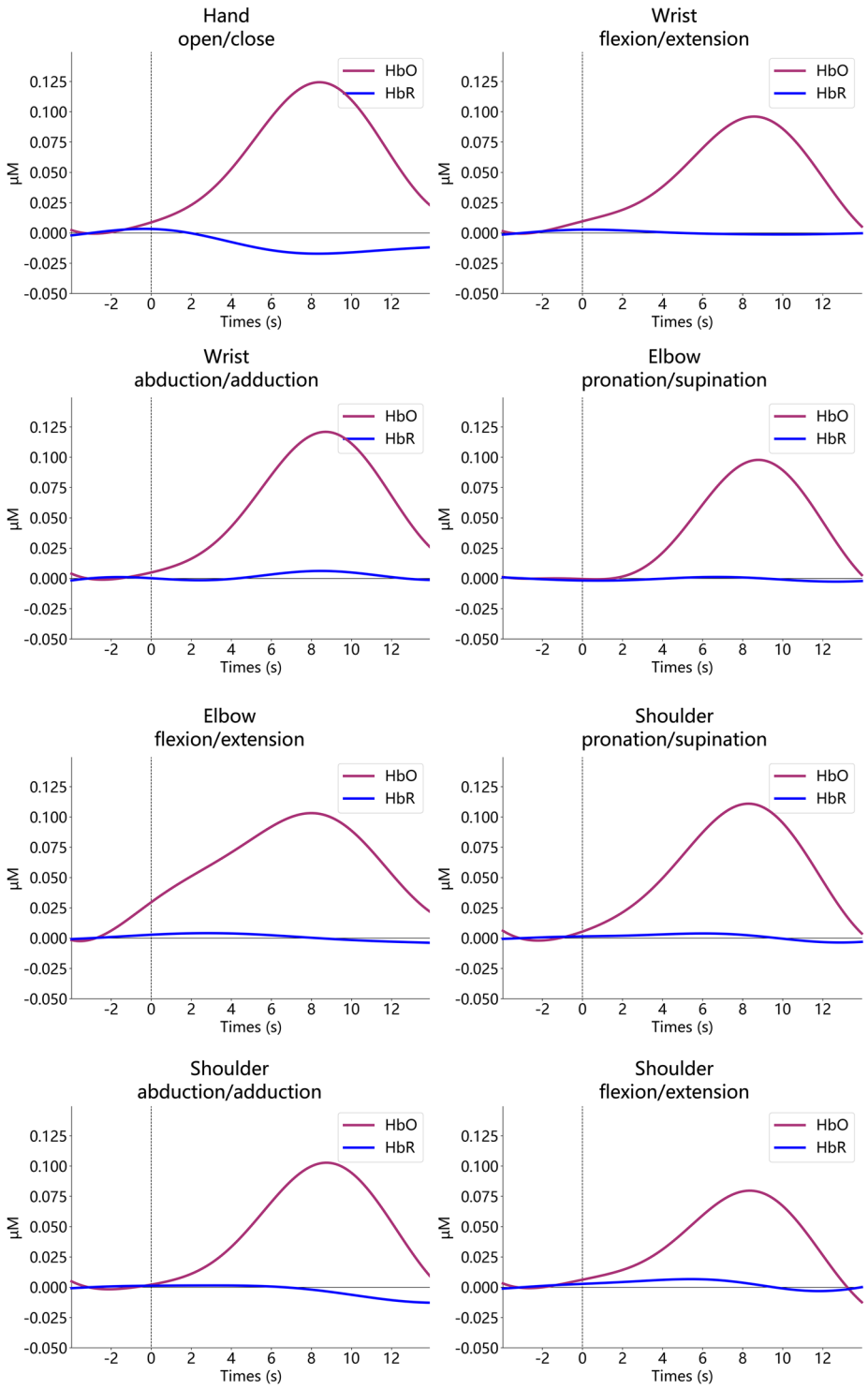

Fig. 7 Averaged concentration changes of HbO and HbR across 18 subjects for 8 MI tasks.

also sorted in descending order. Highest classification performance (61.87%) can be found in the classification of MI tasks between hand and shoulder. In addition, most of the top-10 results are from the classification of hand-shoulder and wrist-shoulder tasks. Also, lower classification results are observed in the classification of hand-wrist, wrist-elbow, and elbow-shoulder tasks. It is indicated that the distribution of classification accuracy in different tasks for fNIRS data is similar with that for EEG data. In addition to conventional machine learning-based methods, future improvements can be achieved by deep learning-based methods equipping with the attention mechanism[34], which are helpful for improving the decoding performance with collected fNIRS data.

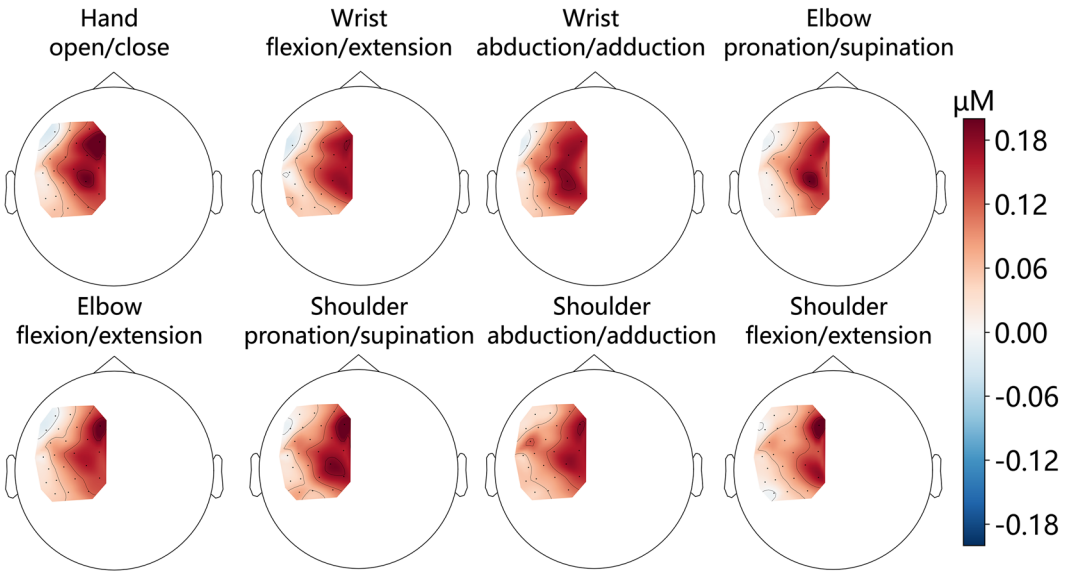

Fig. 8 Averaged topographical maps of concentration of HbO across 18 subjects for 8 MI tasks.

Tasks	Acc. (%)	Tasks	Acc. (%)	Tasks	Acc. (%)	Tasks	Acc. (%)
HOC/SAA	61.87	WAA/SAA	57.54	SPS/SAA	56.00	EFE/SPS	54.52
HOC/SFE	61.03	EPS/SFE	57.01	WFE/SPS	55.78	SAA/SFE	54.10
HOC/SPS	59.90	WAA/SPS	57.00	EPS/SAA	55.76	WAA/EPS	53.68
WFE/SAA	59.67	HOC/WFE	56.91	WFE/WAA	55.68	WFE/EFE	53.25
WFE/SFE	58.96	HOC/EFE	56.65	EFE/SAA	55.62	EPS/EFE	52.99
WAA/EFE	58.02	HOC/WAA	56.62	EPS/SPS	54.73	SPS/SFE	52.79
WAA/SFE	57.95	EFE/SFE	56.20	WFE/EPS	54.70	HOC/EPS	52.35

Table 2. The mean accuracy of temporal features (mean and slope) with SVM on fNIRS data of 18 subjects in an intra-subject 5-fold cross-validation experiment in 2-class scenario. Acc. means accuracy. "A/B" stand for the classification between task A and B. HOC, WFE, WAA, EPS, EFE, SPS, SAA, and SFE stand for hand open/close, wrist flexion/extension, wrist abduction/adduction, elbow pronation/supination, elbow flexion/extension, shoulder pronation/supination, shoulder abduction/adduction, and shoulder flexion/extension, respectively.

Usage Notes

Raw recordings of simultaneously collected EEG-fNIRS can be accessed from the repository at "https://doi.org/10.6084/m9.figshare.24123303". Users can choose to use the EEGLAB toolbox (https://sccn.ucsd.edu/eeglab/index.php) in MATLAB or the MNE-Python library (https://mne.tools/stable/index.html) in Python to load and analyze EEG data. For loading and analyzing fNIRS data, it is recommended to use the MNE-Python library or the nirsLAB provided by NIRx (https://www.nitrc.org/projects/fnirs_downstate/). Regarding the decoding process, the scikit-learn (https://scikit-learn.org/stable) and PyTorch (https://pytorch.org/) library can be used. The codes based on these libraries are available in the "Codes" directory of the repository. (Note that these codes were verified under scikit-learn 1.2.2, PyTorch 1.11, and MNE-Python 1.3.1).

Code availability

The MATLAB script EEG_load_and_plot.m was used for loading EEG data and plotting the time-frequency and topographical maps. The Python script fNIRS_load_and_plot.py was used for loading fNIRS data and plotting the time courses and topographical maps. The Python scripts EEG_decoding.py and fNIRS_decoding.py were used for loading and decoding EEG and fNIRS data, respectively. These scripts are publicly available in the "Codes" folder accompanied with the data in the repository. Also, we released the codes in GitHub at "https://github.com/Bill-Chen-BJ/FJMI_EEG_fNIRS".

Received: 19 September 2023; Accepted: 28 May 2025;
Published online: 06 June 2025

References

1. Willett, F. R. *et al*. High-performance brain-to-text communication via handwriting. *Nature* **593**, 249–254 (2021).
2. Zhang, D., Li, H. & Xie, J. MI-CAT: A transformer-based domain adaptation network for motor imagery classification. *Neural Netw.* **165**, 451–462 (2023).

3. Yi, W. *et al*. EEG feature comparison and classification of simple and compound limb motor imagery. *J. NeuroEngineering Rehabil.* **10**, 106 (2013).
4. Edelman, B. J., Baxter, B. & He, B. EEG source imaging enhances the decoding of complex right-hand motor imagery tasks. *IEEE Trans. Biomed. Eng.* **63**(1), 4–14 (2016).
5. Ma, X., Qiu, S., Wei, W., Wang, S. & He, H. Deep channel-correlation network for motor imagery decoding from the same limb. *IEEE Trans. Neural Syst. Rehabil. Eng.* **28**(1), 297–306 (2019).
6. Yong, X. & Menon, C. EEG classification of different imaginary movements within the same limb. *PloS one* **10**(4), e0121896 (2015).
7. Liao, W., Li, J., Zhang, X. & Li, C. Motor imagery brain–computer interface rehabilitation system enhances upper limb performance and improves brain activity in stroke patients: A clinical study. *Front. Hum. Neurosci.* **17**, 1117670 (2023).
8. Yang, L. *et al*. A multi-feature fusion decoding study for unilateral upper-limb fine motor imagery. *Math. Biosci. Eng.* **20**(2), 2482–2500 (2023).
9. Qiu, W., *et al* The Paradigm Design of a Novel 2-class Unilateral Upper Limb Motor Imagery Tasks and its EEG Signal Classification. In *2021 43rd Annual International Conference of the IEEE Engineering in Medicine & Biology Society (EMBC)*, 152–155 (2021).
10. Vuckovic, A. & Sepulveda, F. Delta band contribution in cue based single trial classification of real and imaginary wrist movements. *Med. Biol. Eng. Comput.* **46**, 529–539 (2008).
11. Chu, Y. *et al*. Decoding multiclass motor imagery EEG from the same upper limb by combining Riemannian geometry features and partial least squares regression. *J. Neural Eng.* **17**(4), 046029 (2020).
12. Zhao, D., Tang, F., Si, B. & Feng, X. Learning joint space–time–frequency features for EEG decoding on small labeled data. *Neural Netw.* **114**, 67–77 (2019).
13. Suwannarat, A., Pan-Ngum, S. & Israsena, P. Comparison of EEG measurement of upper limb movement in motor imagery training system. *Biomed. Eng. Online* **17**(1), 1–22 (2018).
14. Guan, S., *et al* Multi-class Motor Imagery Recognition of Single Joint in Upper Limb Based on Multi-domain Feature Fusion. *Neural Process. Lett*. 1–19 (2023).
15. Gwon, D. *et al*. Review of public motor imagery and execution datasets in brain-computer interfaces. *Front. Hum. Neurosci.* **17**, 1134869 (2023).
16. Tangermann, M. *et al*. Review of the BCI competition IV. *Front. Neurosci.* **6**, 00055 (2012).
17. Lee, M. H. *et al*. EEG dataset and OpenBMI toolbox for three BCI paradigms: An investigation into BCI illiteracy. *GigaScience* **8**(5), giz002 (2019).
18. Ofner, P., Schwarz, A., Pereira, J. & Müller-Putz, G. R. Upper limb movements can be decoded from the time-domain of low-frequency EEG. *PloS One* **12**(8), e0182578 (2017).
19. Ma, X., Qiu, S. & He, H. Multi-channel EEG recording during motor imagery of different joints from the same limb. *Sci. data* **7**(1), 191 (2020).
20. Bi, J., Chu, M., Wang, G. & Gao, X. TSPNet: a time-spatial parallel network for classification of EEG-based multiclass upper limb motor imagery BCI. *Front. Neurosci.* **17**, 1303242 (2023).
21. Chiarelli, A. M., Zappasodi, F., Di Pompeo, F. & Merla, A. Simultaneous functional near-infrared spectroscopy and electroencephalography for monitoring of human brain activity and oxygenation: a review. *Neurophotonics* **4**(4), 041411 (2017).
22. Zhang, Y., Qiu, S. & He, H. Multimodal motor imagery decoding method based on temporal spatial feature alignment and fusion. *J. Neural Eng.* **20**(2), 026009 (2023).
23. Schirrmeister, R. T. *et al*. Deep learning with convolutional neural networks for EEG decoding and visualization. *Hum. Brain Mapp.* **38**(11), 5391–5420 (2017).
24. Shin, J. *et al*. Open access dataset for EEG + NIRS single-trial classification. *IEEE Trans. Neural Syst. Rehabil. Eng.* **25**(10), 1735–1745 (2016).
25. Gramfort, A. *et al*. MEG and EEG data analysis with MNE-Python. *Front. Neurosci.* **7**(267), 1–13 (2013).
26. Fazli, S. *et al*. Enhanced performance by a hybrid NIRS–EEG brain computer interface. *NeuroImage* **59**(1), 519–529 (2012).
27. Yi, W.-B., Chen, J.-M. & Wang, D. *figshare* https://doi.org/10.6084/m9.figshare.24123303 (2023).
28. Pfurtscheller, G. & Da Silva, F. L. Event-related EEG/MEG synchronization and desynchronization: basic principles. *Clin. Neurophysiol.* **110**(11), 1842–1857 (1999).
29. He, C., Liu, J., Zhu, Y. & Du, W. Data augmentation for deep neural networks model in EEG classification task: a review. *Front. Hum. Neurosci.* **15**, 765525 (2021).
30. Ma, X., Qiu, S. & He, H. Time-distributed attention network for EEG based motor imagery decoding from the same limb. *IEEE Trans. Neural Syst. Rehabil. Eng.* **30**, 496–508 (2022).
31. Zheng, W., Yan, L. & Wang, F. Y. Two birds with one stone: Knowledge-embedded temporal convolutional transformer for depression detection and emotion recognition. *IEEE Trans. Affect. Comput.* **14**(4), 2595–2613 (2023).
32. Kaiser, V. *et al*. Cortical effects of user training in a motor imagery based brain–computer interface measured by fNIRS and EEG. *NeuroImage* **85**, 432–444 (2014).
33. Gao, Y., Jia, B., Houston, M. & Zhang, Y. Hybrid EEG-fNIRS Brain Computer Interface based on Common Spatial Pattern by using EEG-informed General Linear Model. *IEEE Trans. Instrum. Meas.* **72**, 4006110 (2023).
34. Zhang T., Li Q., Wen J., Chen C. P. Enhancement and optimisation of human pose estimation with multi-scale spatial attention and adversarial data augmentation. *Inf. Fusion* 102522 (2024).

Acknowledgements

This work was supported by the Natural Science Foundation of China under Grant 62006014, U2441253, and 12275295, the Postdoctoral Fellowship Program of China Postdoctoral Science Foundation under Grant Number GZC20230189, and the Project of Construction and Support for High-level Teaching Teams of Beijing Municipal Institutions.

Author contributions

W. Yi, J. Chen, and D. Wang designed this study. W. Yi, J. Chen, M. Xu, F. Li, S. Wu, J. Qian conducted the experiments. W. Yi, J. Chen, and X. Hu performed the data analysis. W Yi and J. Chen wrote the manuscript. All authors reviewed the manuscript and approved the final manuscript.

Competing interests

The authors declare no competing interests.

Additional information

Correspondence and requests for materials should be addressed to W.Y. or D.W.